SCIENTIFIC REPORTS

OPEN

SUBJECT AREAS:
GEOLOGY
TECTONICS
MINERALOGY
SEISMOLOGY

Received
24 October 2012

Accepted
28 January 2013

Published
15 February 2013

Correspondence and requests for materials should be addressed to A.P. (alina.polonia@ismar.cnr.it)

Mediterranean megaturbidite triggered by the AD 365 Crete earthquake and tsunami

Alina Polonia[1], Enrico Bonatti[1,2], Angelo Camerlenghi[3], Renata Giulia Lucchi[3], Giuliana Panieri[1] & Luca Gasperini[1]

[1]ISMAR-CNR (Istituto di Scienze Marine), Via Gobetti 101, 40129 Bologna, Italy, [2]Lamont-Doherty Earth Observatory, 61 Rte 9w, Palisades, NY 10964, United States, [3]OGS (Istituto Nazionale di Oceanografia e di Geofisica Sperimentale), Borgo Grotta Gigante 42/C, 34010, Sgonico (TS), Italy.

Historian Ammianus Marcellinus documented the devastating effects of a tsunami hitting Alexandria, Egypt, on July 21, AD 365. "The solidity of the earth was made to shake … and the sea was driven away. The waters returning when least expected killed many thousands by drowning. Huge ships… perched on the roofs of houses… hurled miles from the shore….". Other settlements around the Mediterranean were hit at roughly the same time. This scenario is similar to that of the recent Sumatra and Tohoku tsunamis. Based on geophysical surveys and sediment cores from the Ionian Sea we show that the 20–25 m thick megaturbidite known in the literature as Homogenite/Augias was triggered not by the Santorini caldera collapse but by the 365 AD Cretan earthquake/tsunami. An older similar megaturbidite was deposited after 14.590 ± 80 yr BP, implying a large recurrence time of such extreme sedimentary events in the Mediterranean Sea.

Extreme submarine geo-hazards, such as strong earthquakes, tsunamis, volcanic eruptions and submarine landslides have affected repeatedly the circum Mediterranean highly populated coastal regions. A record of these past events can be provided by large-volume turbidites or megaturbidites[1], detected in the marine sedimentary record. Megaturbidites can be triggered by ground acceleration from seismic events[2], impact on the seafloor of tsunami waves[3], volcanic activity[4], sea-level changes[5], gas hydrate phase changes[6] or a combination of any of these processes.

Megaturbidites have been identified in the Ionian basin, a deep and thickly sedimented relict of the Tethis Ocean[7]. It contains sedimentary sequences spanning from Jurassic to the present, that includes, in its upper part, about 2 km of Messinian (Late Miocene) evaporites overlain by Plio-Quaternary sediments[8]. The basin is located between the tectonically active Calabria and Hellenic subduction zones (to the North and to the East respectively), the Malta escarpment to the West and the African plate passive margin to the South (Fig. 1).

Post evaporitic deposits consist of alternating pelagic sediments (including sapropels and tephras) and turbidites. Turbidites and megaturbidites are prevalent in the flat deep basin floor (Ionian and Sirte abyssal plains) and on the rims of the Calabrian and Mediterranean ridges, while hemipelagic sedimentation prevails on topographic highs[9].

The recentmost megaturbidite, described for the first time in 1975[10] was named either "Homogenite"[3], or "Augias homogenite"[11] or "Augias turbidite"[12]. The term Homogenite was introduced to indicate the apparently homogeneous and structureless, very-fine grained sediments forming the uppermost part of the megabed. "Homogenite" is therefore a descriptive term initially used to indicate a deposit having sedimentary characteristics similar to the "unifites"[13].

The Homogenite has been detected from different tectonic and physiographic settings[14]. Type A Homogenite[15] refers to pelagic turbidites of local origin, up to seven metre-thick, deposited in small perched basins of the Calabrian and Western Mediterranean Ridges, deriving from sediment liquefaction and resuspension triggered by the repeated passage of a tsunami wave. Type B Homogenite refers to a terrigenous megaturbidite, in places up to 25 m thick[15,16], recovered in the Sirte and central Ionian abyssal plains and in the Western Herodotus Trough. It was triggered by the tsunami wave hitting the Northern African shallow water shelf and coastline. The exceptional thickness of Type B Homogenite prevented recovery of its coarse-grained base in most cases. The Augias turbidite[12] refers to Type B Homogenite[15] as discussed in ref 17. In order to avoid misunderstanding, in this paper we refer to the Homogenite/Augias Turbidite as HAT.

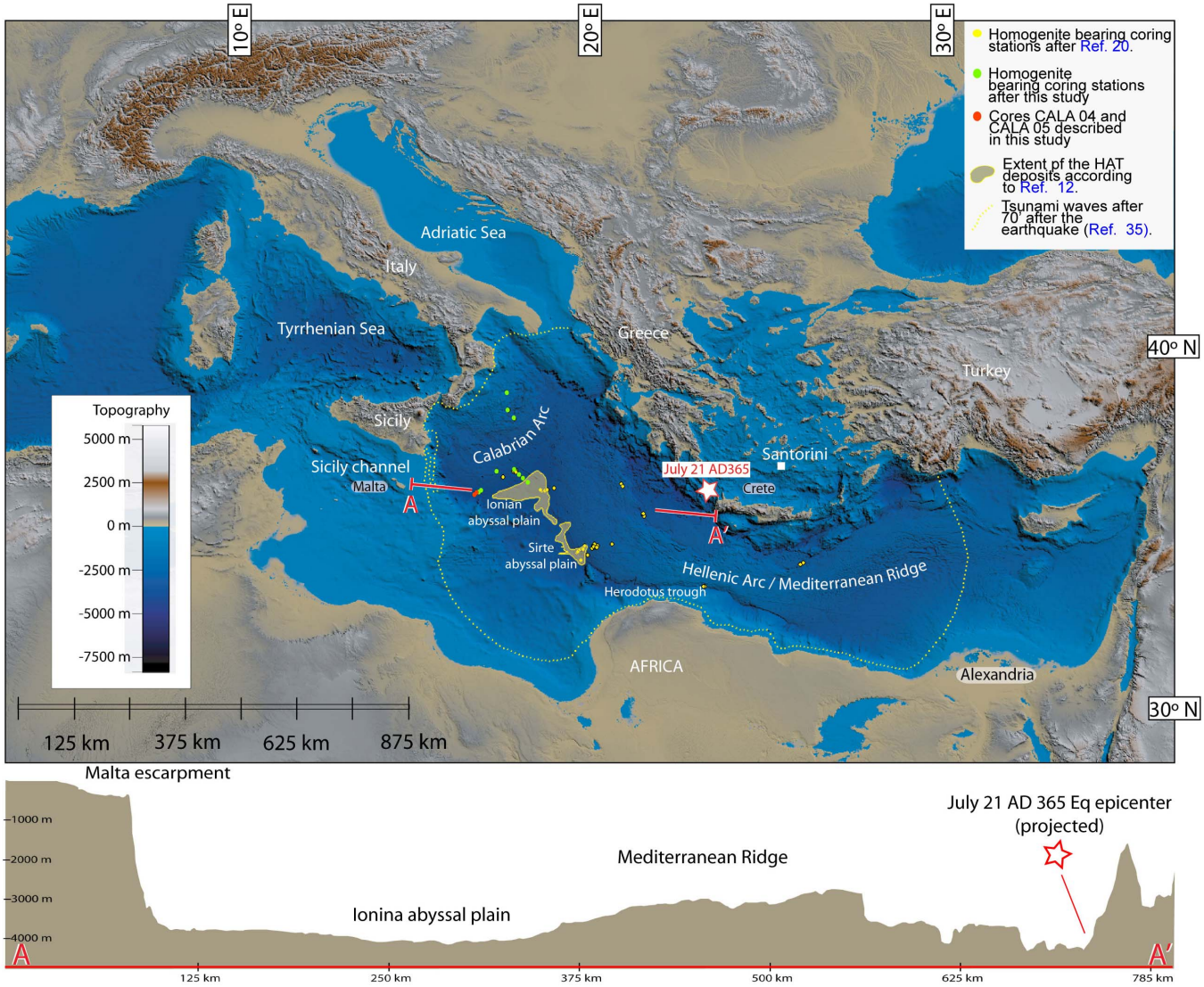

Figure 1 | Shaded relief map of topography/bathymetry of the central and eastern Mediterranean Sea. Shaded relief map of topography/bathymetry of the central and eastern Mediterranean Sea: Global Bathymetry and Elevation Data from SRTM30_PLUS (Becker et al., 2009). Yellow areas indicate the extent of HAT deposits according to ref 12. Yellow dots represent homogenite bearing coring stations after ref 20. Green dots represent homogenite bearing gravity cores after this study while red dots represent the two gravity cores described in this manuscript (cores CALA 04 and CALA 05). Section A-A′ is a bathymetric profile from the AD 365 epicentre to the Malta escarpment, crossing coring stations CALA 04 and −05. Bottom: bathymetric profile A-A′ that shows the very steep topographic gradient (up to 30°) of the Malta Escarpement with a large vertical displacement of the seafloor (>2000 m) relative to the basin floor. The top of the escarpment represents the edge of a wide continental shelf in the Sicily Channel. Dotted yellow line represents tsunami waves after 70′ after the earthquake[34].

The stratigraphic position of the HAT, defined in tens of sediment cores above the regional stratigraphic marker sapropel S1, has been interpreted as evidence for deposition in a single, basin-wide event capable to put into suspension simultaneously sediment at a basin-wide scale. To date, the HAT is a unique example of the multiple effects that a tsunami wave can produce on deep sea sedimentation in a Mediterranean type basin such as the Ionian Sea. Absence of absolute dating of the HAT and of a detailed chronostratigraphy of the deposits above and below the HAT, have allowed different correlations with known historic natural catastrophes in the Eastern Mediterranean region.

The original hypothesis, put forward by[3,11,18] and elaborated in several other researche articles[18–21] for nearly 30 years, attributed the HAT to the 3500 yr BP Minoan eruption of Santorini and related tsunamis originated in the Aegean Sea. This chronology was based on the linear extrapolation of sedimentation rate between the top of sapropel S1 (8000 yr B.P.) and the seafloor assuming no erosion was caused by deposition of Type A Homogenites.

The improvement of tsunami modeling led to question the effectiveness of the tsunami wave generated by the Santorini caldera collapse, especially outside the Aegean Sea, and to propose that the homogenite was generated by a tsunami driven by the collapse of the eastern flank of the Etna Volcano[22]. This reconstruction was criticized[23] based on the incongruent chronology between the Etna flank collapse, the Santorini caldera collapse, and the age of the sapropel S1. This led to the suggestion that the Homogenite might be related to a 365 AD major earthquake in Crete[23]. No novel data nor detailed geological or radiometric data analysis accompanied this hypothesis.

We present here the results of acoustic surveys of the HAT in the Ionian Sea, as well as HAT's mineralogy, micropaleontology, elemental and isotopic geochemistry and radiocarbon dating, based on studies of sediment cores we collected from the Ionian seafloor.

Guided by online sub-bottom CHIRP seismic data, we were able, in fact, to sample the top and base of the megaturbidite in different sedimentary basins of the Ionian Sea by carefully selecting sites where it has its minimum thickness.

The objective is to identify the event or events that triggered the deposition of the HAT, and to assess the recurrence time of such major catastrophic events in the Mediterranean.

Results

Sub-bottom acoustic profiles of the HAT. High resolution sub-bottom CHIRP seismic profiles identified the HAT in the Ionian abyssal plain as a laterally continuous, acoustically transparent near surface layer (Fig. 2 and Supplementary S1). It has a uniform thickness of about 15 m in the deep basin while it pinches out to a few meters towards the basin's margins. The HAT correlates on sub-bottom profiles, with the Augias turbidite described in previous works[24,25] (see Supplementary S1).

The HAT is not limited to the abyssal plain (Type B Homogenite[15] and Augias turbidite[12]); we can acoustically document the HAT also in confined perched basins on the continental slope both of the outer Calabrian Arc accretionary wedge (Type A Homogenite[15]) and, for the first time, in the inner portions of the subduction complex, about 100 km from the Calabrian coastline (Fig. 1), where its thickness ranges from 1 to 3 m. Other thick acoustically transparent layers have been detected beneath the HAT (Fig. 2b and Supplementary S1) that may be correlated to the DTL (Deep Transparent Layer) and TTL (Thick Transparent Layer) of ref 25.

Composition of the HAT. We detected the HAT in 12 of the 19 cores retrieved from the abyssal plain and slope basins (Fig. 1). We selected core CALA 05 for a high resolution multidisciplinary study while radiometric dating has been performed both on CALA 05 and CALA 04 (see section on methods).

Core CALA 05 consists of thin pelagic sediments (yellow units in Fig. 3) interbedded with sandy and silty turbidites. Turbidite beds were identified based on: (a) sharp colour changes; (b) sharp basal boundaries, with coarse sandy basal units; (c) graded bedding; and (d) displaced foraminifera assemblages.

The HAT is located stratigraphically above sapropel S-1[26] and below three terrigenous sandy/silty turbidites (each of them about 20–30 cm thick) possibly linked to three major historical Italian earthquakes[27] (i.e. 1908, 1693 and 1169). Centimetric thick turbidite beds interbedded with cm-thick pelagic units separate the HAT from the underlying sapropel bed S-1 (Fig. 3). The older stratigraphic sequence below sapropel S1, contains several other terrigenous turbidites characterized by sharp/erosive bases and topped by thin, cm-thick pelagic intervals (Fig. 4).

The HAT is 1.84 m thick in core CALA 05; a complex depositional sequence is displayed by X-ray images, grain-size distribution (Fig. 3) and composition (Supplementary S2 and Fig. 5). The base of the megabed shows a sharp increase in sand content (Fig. 3). The sand consists of an heterogeneous mixture of detrital mineral grains (plagioclase, clynopiroxene, amphibole, basaltic glass, feldspar, carbonates, pyrite incrustations) and biogenic components (Supplementary S2).

The HAT stands out in the stratigraphic log of Fig. 3 because of strong and peculiar geochemical signatures, including high Ca and Sr content, due to abundance of calcareous components. Its high value of Corg/Ntot suggests a continental origin of the organic matter (OM)[28].

Sedimentology and geochemistry of the core identified 5 major turbidite units (Fig. 3). Micropaleontological and mineralogical analysis further confirmed that these units have different composition and sources (Supplementary S2 and S3). The 3 cm thick basal Unit I of the HAT is normally graded (Fig. 3) with a sharp sandy base. The upper part of this interval is truncated by the main erosive base of the HAT containing flute-like erosive basal structures, implying high-energy hydrology of the turbidity flow.

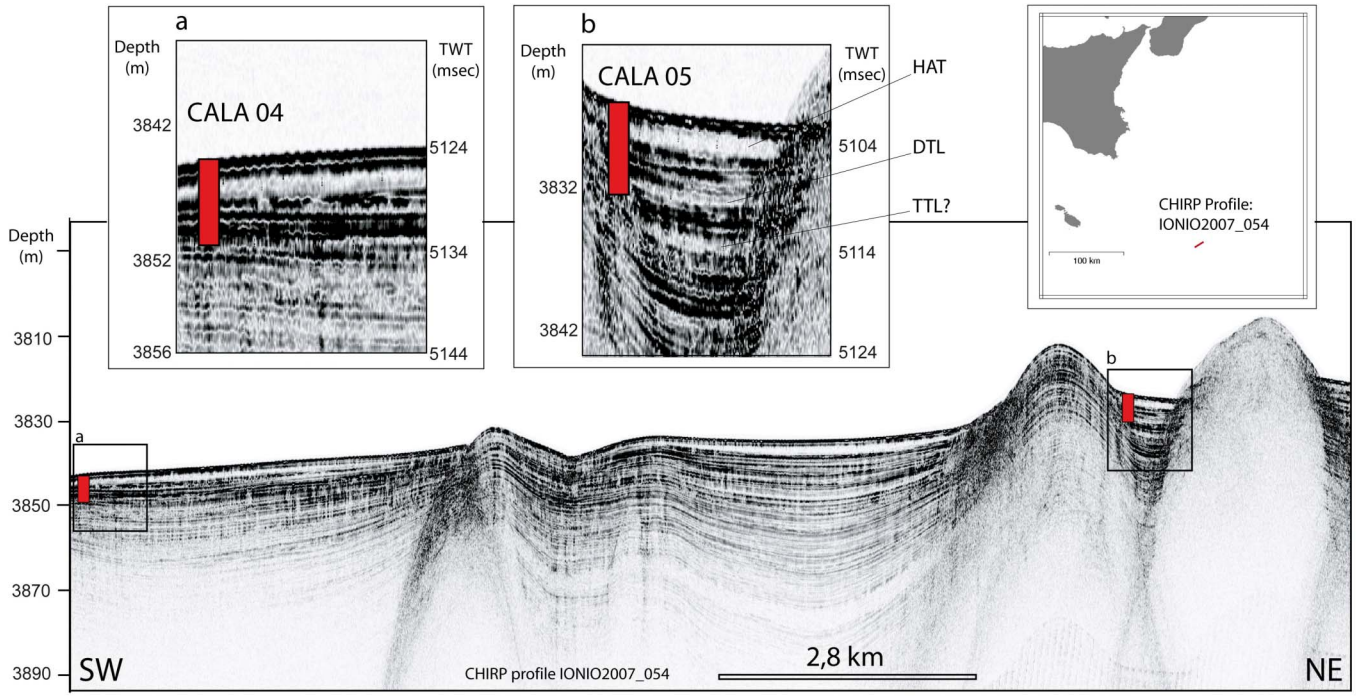

Figure 2 | Sub-bottom CHIRP profile across the gravity cores. Sub-bottom CHIRP profile across the gravity cores described in this work (see Fig. 1 for location of the gravity cores represented by the red circles). The profile crosses the transition between the undeformed abyssal plain to the SW and the outer accretionary wedge to the NE. Gravity cores CALA 04 and CALA 05 are represented on the CHIRP profile. a: zoom of the CHIRP profile on the CALA 04 coring station. b: zoom of the CHIRP profile on the CALA 05 coring station. c: location of CHIRP seismic profile. HAT: Homogenite/Augias turbidite. DTL: Deep Transparent Layer. TTL: Thick Transparent Layer.

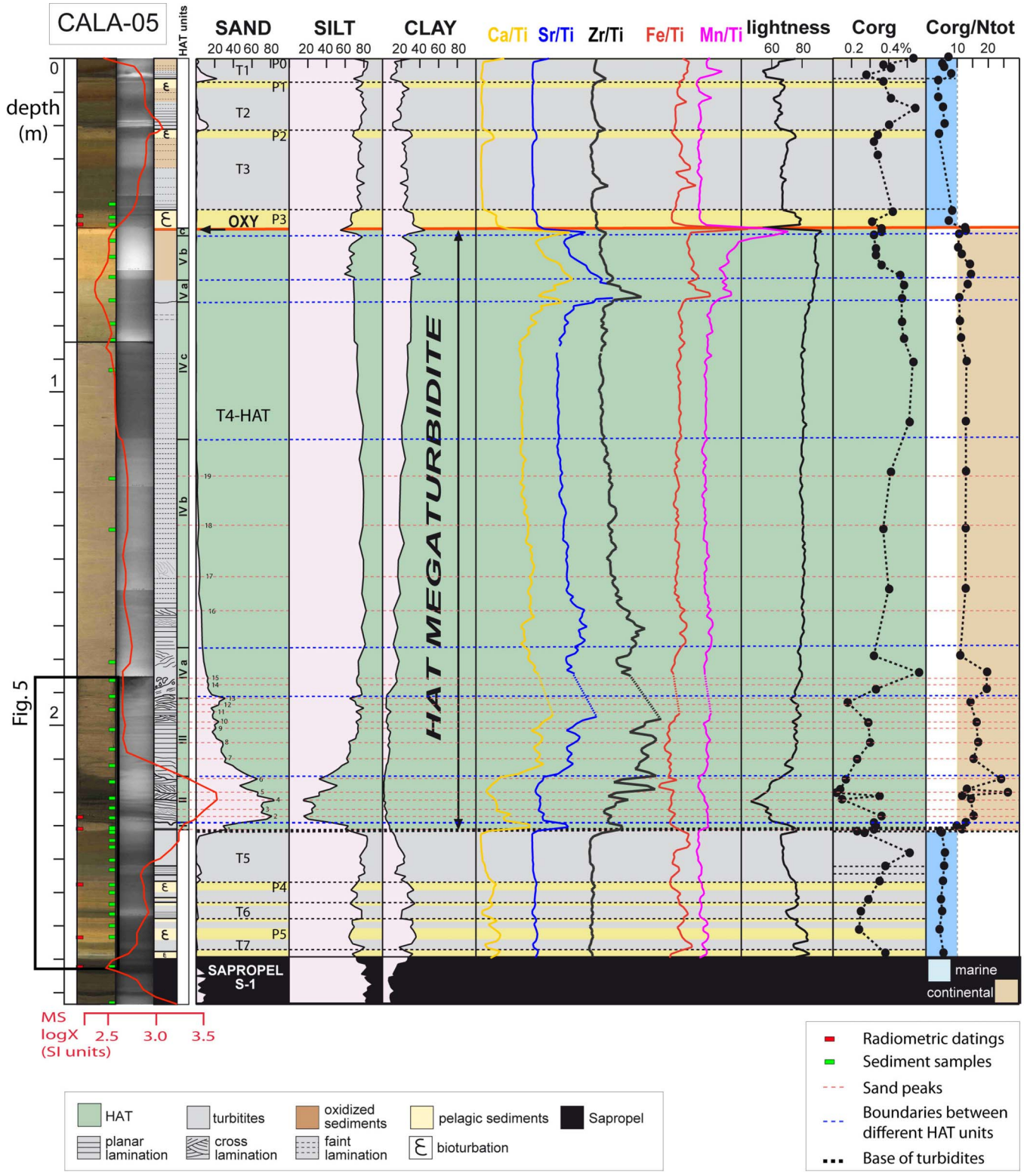

Figure 3 | Photograph, X-ray image, sedimentary facies, grain size and geochemical data of core CALA 05. From left to right: Photograph with overprinted the magnetic susceptibility profile, X-ray image, sedimentary facies, grain-size, major XRF geochemical elements, lightness profiles and OM content. Recognized turbidites (T1-T7), pelagic units (P0-P5), sapropel S1 are indicated. Numbered (from 1 to 19) red dotted lines represent sand peaks in the different HAT units. Analysed samples and ^{14}C dated samples are indicated by green and red rectangles respectively. MS: Magnetic Susceptibility.

The 15 cm thick dark brown sandy Unit II is characterized by 2–3 cm inversely graded basal sand with alternating mm-thick light and dark levels containing abundant biogenic components (Supplementary 2). Above this interval the sequence is normally graded, although we distinguished 5 peaks of increased sand concentration, each marked by an increase of Zr and Fe content. X-ray analyses of Unit II reveals a complex pattern of alternating planar and cross-laminations separated by sharp surfaces marked by

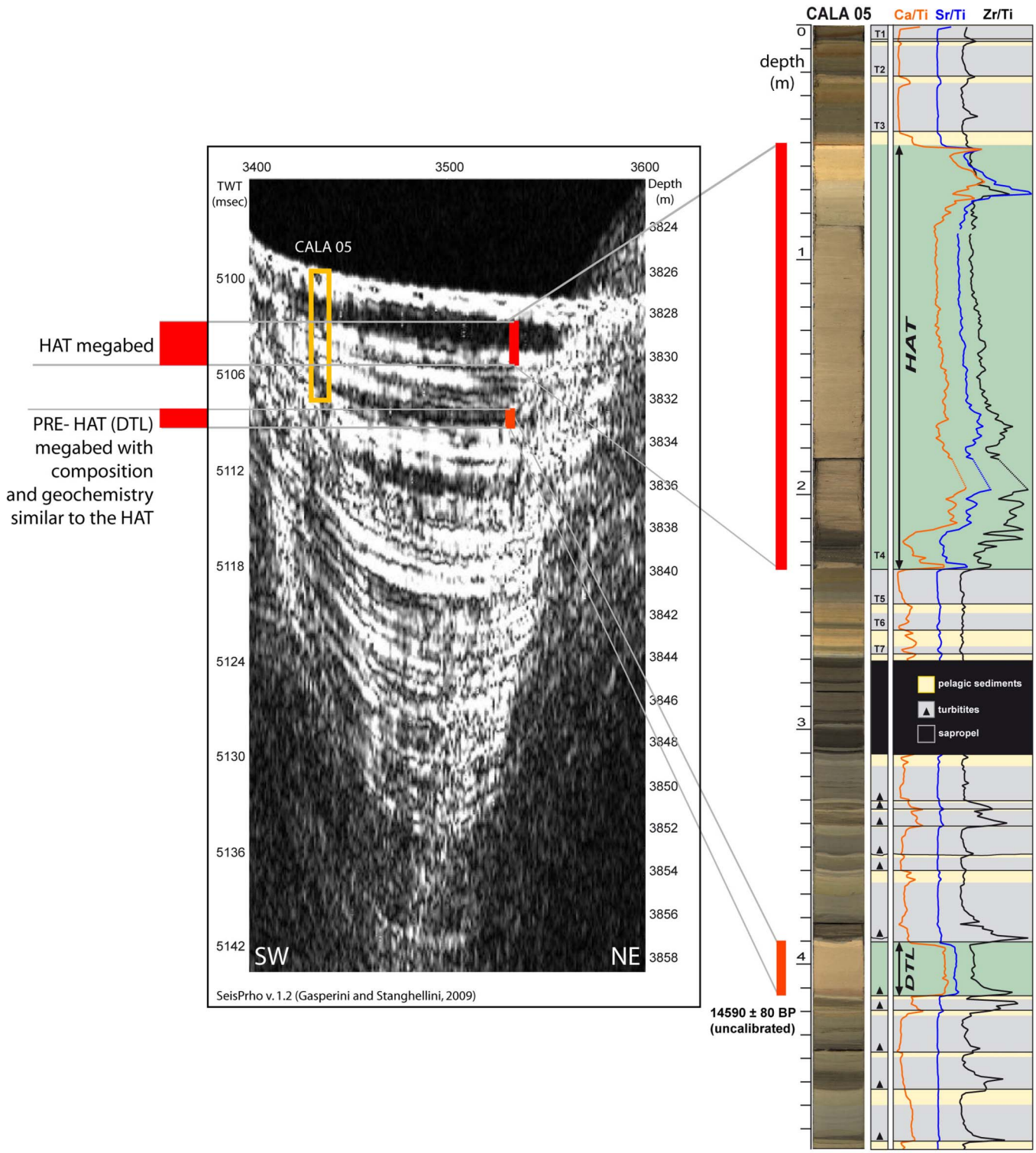

Figure 4 | Two similar megaturbidites revealed by CHIRP data and core CALA 05. The HAT and DTL (Deep Transparent Layer[25]) megaturbidites are highlighted in the gravity core as well as in the CHIRP profile. They stand out in the CHIRP profile because of the low reflectivity facies related to the upper rather homogeneous part of the megabed; they are characterized by strong and peculiar geochemical signatures: i.e., a high content of Ca and Sr, suggesting abundance of calcareous components. The DTL composition suggests a similar source region as the HAT megaturbidite. Biogenic components of the DTL include: planktonic foraminifera (from Holocene to Cretaceous formations); benthic foraminifera (from inner shelf, epiphyte and abundant Miliolids); ossicles of holoturoidea; spiculae of Demospongiae; Echinoids spiculae; shell hash; bryozoans; fresh plant remnants. Source region: Malta escarpment, Sicily channel and Greek margins.

increasing grain size (Fig. 3). In some cases, amalgamated intervals of cross-laminated sediments show opposite dipping trends, suggesting reversal of flow direction.

The sharp and irregular base of Unit III is marked by a colour change and a decrease in sand content. Planar and cross-laminations are present, as well as grain size fluctuations with at least 6 sandy peaks. This unit shows a relative enrichment in OM.

Unit IV is limited at the base by a sharp contact separating the sand-silt parallel and cross laminations of unit III from a depositional sequence that includes the following sub-units: a) a basal debrite (mud chips visible on the Xray images in a homogenous mud matrix); b) alternation of cross, planar and convoluted/cross laminated layers; c) texturally uniform sediments with faint, sand free, laminations.

Unit V consists of structureless, very-fine grained sediments with an upward decrease of OM content. At the base, unit Va shows a sharp basal boundary visible on X-ray images with low magnetic susceptibility and geochemical anomalies; unit Vb shows an abrupt increase in clay content and is marked by colour variation; the uppermost unit Vc corresponds to geochemical anomalies and evidences of bacteria activity. A millimetric black and reddish horizon is present at the top of the HAT (Figs. 3 and 5a), enriched in Fe and Mn and with abundant Fe/Mn micro-nodules. This horizon could represent a diagenetic red-ox front marking the top of the turbidite[29], caused by mobilization of Fe and Mn within the turbidite following the development of reducing condition induced by the rapid sediment accumulation. The fine-grained upper part of the HAT has an increased concentration of organic carbon whose bacterial oxidation (Fig. 3) may lead to reduction of Fe and Mn oxides and sulphates.

The HAT differs from the non-sapropelic pelagic intervals for its higher C_{org}/N_{tot} ratio (Fig. 3), suggesting a prevailing terrestrial origin of the organic matter. Highest C_{org}/N_{tot} ratios are found in the lowermost coarsest part (Units I, II, and III), which includes abundant land-derived plant debris. Conversely, the enrichment of clay particles in the fine-grained fraction favours the absorption of ammonia, thus decreasing the C_{org}/N_{tot} ratio.

Only another decimetric thick carbonatic-sandy turbidite was recovered at the base of the core (Fig. 4). Correlation with CHIRP data (Figs. 2, 4 and Supplementary S1) suggests it may be the DTL layer[25] (Fig. 4 and Supplementary S1). The HAT and DTL stand out in the CHIRP profiles (Fig. 4 and Supplementary S1) because of the low reflectivity facies at the upper rather homogeneous part of the megabeds. Both these turbidites are characterized by strong and peculiar geochemical signatures, including a high content of Ca and Sr, suggesting abundance of calcareous components. The DTL composition suggests a similar source region as the HAT megaturbidite (Fig. 4).

Radiocarbon dating of the HAT. Radiocarbon ages were obtained from planktonic foraminifera above and beneath the HAT, within the coarse base and at different stratigraphic levels in two cores that contain the entire HAT sequence, CALA 04 and CALA 05 (Table 1 and Fig. 5).

The ages we obtained above the top of the turbidite were corrected by the time interval corresponding to the thickness of pelagic sedimentation separating the top of the HAT and the dated level. Pelagic sedimentation rates in the two cores have been estimated from two samples spaced 2 cm apart within pelagic unit P3 above the HAT in core CALA 05, and 4 cm apart in core CALA 04 (Fig. 5). The C14 ages of these samples suggest average rates of pelagic-normal sedimentation in the deep Ionian Sea of 0,068 mm/yr (0,054–0,083 mm/yr) in core CALA 05 and 0,097 mm/yr (0.095–0,100 mm/yr) in core CALA 04, in good agreement with the sedimentation rate of 0.05–0.1 mm/yr reported by ref 9. We derive that, under "normal" pelagic conditions, the time interval introduced by sampling above the top of the megaturbidite, is 110 ± 46 and 140 ± 46 years, respectively, for each cm above the top.

Radiometric dating (Table 1 and Fig. 5) suggest that:

1) The sample dated 3 cm above the HAT in core CALA 04 (1860 ± 30 uncalibrated) was deposited within the calibrated time range AD 598-781. To obtain the age of HAT we have to subtract the time interval corresponding to the 3 cm of pelagic sedimentation (330 ± 79 years). The time-window for HAT deposition in core CALA 04 is thus AD 189-530.
2) The sample dated 2 cm above the HAT in core CALA 05 (1890 ± 35 uncalibrated) was deposited within the calibrated time range AD 560-762. To obtain the age of the HAT emplacement we need to subtract the time interval corresponding to the 2 cm of pelagic sedimentation (280 ± 65 years); thus, the deposition of HAT in core CALA 05 occurred between 215 and 547 AD.

Assuming that the HAT was deposited simultaneously in the two cores and combining their 14C age intervals, we conclude that the time-window for HAT deposition in the Ionian Sea is AD 215–530.

AMS dating within the coarse sandy basal unit gives much older ages (Table 1) indicating old sediment remobilization by the turbiditic flow. Finally, the lack of about 1000 years in the sedimentary sequence between the top and the base of the HAT, as shown in (Table 1 and Fig 5), implies a basal erosion by HAT emplacement: the absence of pelagic sediments between the HAT and turbidite T5 located just below it, confirm this interpretation.

Age modeling. We have built a depositional model with the OxCal software[30] for core CALA 04 and CALA 05 from the order of deposition of pelagic units and their depth derived subtracting the thickness of the turbidites from the total core (Supplementary 4 and 5). The software identifies mathematically a set of possible ages for each depth point in the sedimentary sequence (Supplementary 6 and 7); turbidite age distributions at 2σ are modelled from their stratigraphic depth of emplacement into the background sequence (Fig. 6). The age intervals derived from the OxCal modelling are large because the P_Sequence is unable to narrow their time interval for lack of an adequate number of ^{14}C dated samples due to the scarcity of in-situ pelagic sediments suitable for dating.

Despite this uncertainty, age modelling allowed us to deduce the following main conclusions: 1) the HAT age distribution is centred on the AD 365 Cretan earthquake (red line in Fig. 6); 2) turbidite T6 (Figs. 3, 4 and 5) is possibly related to the 1627–1600 BC Santorini volcano eruption and collapse[31] (green line in Fig. 6). This implies that the Santorini event might indeed have triggered mass failures in the central Mediterranean, but not the deposition of a megaturbidite.

The recovery in the same core of both the HAT and the Santorini event (T6 turbidite in Figs. 3, 4, 5 and 6) is a key element in support of a younger age of the HAT megaturbidite.

Discussion

The HAT triggering event took place in the time window AD 215–530 and was capable of initiating simultaneously local sediment transport in widely separated sedimentary basins. The lithology, structure and regional occurrence of the HAT place the triggering mechanism within narrow constraints: it affected every basin of the Central Mediterranean but not of the Easternmost Mediterranean (Fig. 1) and its provenance varied in different parts of the basin margins.

The 3500 yr BP Minoan eruption of Santorini and the 7600 yr BP collapse of the flank of the Etna volcano can be excluded since they both occurred outside the HAT time window.

Depending on the triggering mechanism (i.e. earthquake induced direct shaking or near bottom oscillatory currents related to tsunamis), we should consider near field or far field sources; recent numerical simulations[32] indicate that a large Hellenic Arc earthquake can

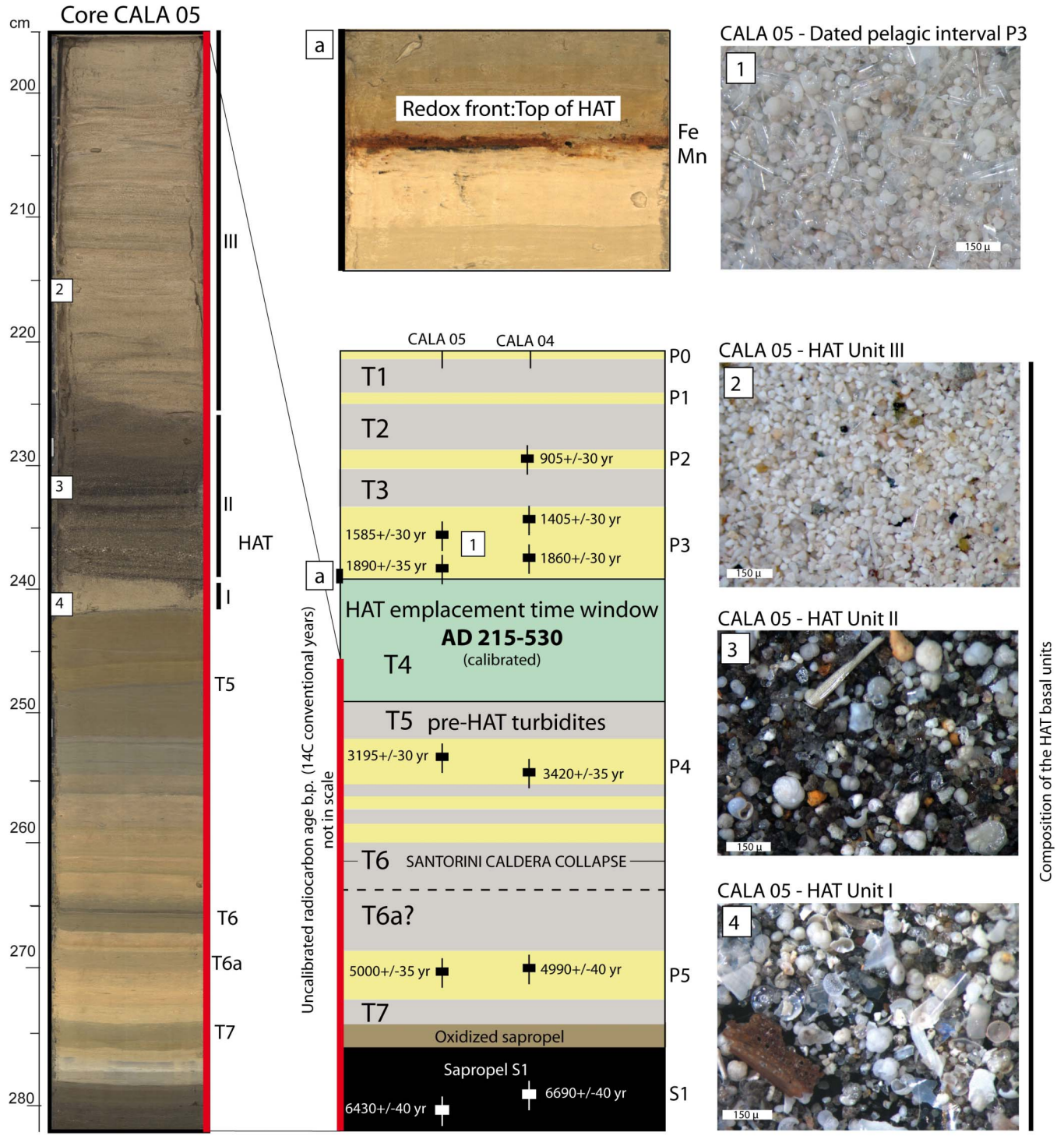

Figure 5 | Radiocarbon ages derived from dating the pelagic intervals. Uncalibrated radiocarbon ages derived from dating the pelagic intervals above and below the megabed in cores CALA 04 and 05. The overlying pelagic samples from the two cores yield a cluster of ages between 215–530 (calibrated). There is a greater scatter in the underlying samples. The best estimate for the emplacement time of the megabed is thus given by the dates of the upper pelagic units. The age of the Santorini caldera collapse and the top of the sapropels S1 are also indicated. a: zoom of the top of the HAT represented by the mm-thick reddish and black level enriched in Fe and Mn and with abundant Fe/Mn micronodules; 1: coloured microphotograph of the sediment fraction of the pelagic unit P3 above the HAT. 2: coloured microphotograph of the sediment fraction within the HAT basal unit III. 3: coloured microphotograph of the sediment fraction within the HAT basal unit II. 4: coloured microphotograph of the sediment fraction within the HAT basal unit I. See Supplementary Material 2 and 3 for details on the composition.

produce a much higher tsunami wave in our working area than tsunami waves originating in closer regions. This implies that possible triggering events (Table 2) include major earthquakes from the regions facing the Ionian Sea, such as the Calabrian Arc subduction system[8,33], the Hellenic Arc[34] or to the Easternmost Mediterranean and northern Africa thrust belts[35,36].

Sicily and Calabria in southern Italy have been struck repeatedly by strong and destructive earthquakes[37] often with

Table 1 | Radiometric ages for cores CALA 04 and CALA 05

1 Core and water depth	2 Sample name and AMS Lab reference	3 Position relative to the HAT	4 Type of sample	5 14C age BP (uncalibrated)	6 Calibrated Age (2σ) according to CALIB REV5.0.2 by ref 54 ΔR = 0	7 HAT age with ΔR = 0: age interpolated on the top of the turbidite	8 Calibrated Age (2σ) with ΔR = 147 ± 33(weighted mean including 2 ΔR in the region)	9 HAT age with ΔR = 147 ± 33: age interpolated on the top of the turbidite
CALA-05 3814 m	CALA-05 V 47–48 Poz-34625	4 cm above the top	Foram	1585 +/− 30	AD 717–894		AD 848–1055	
	CALA 05 V 49–50 Poz-38783	2 cm above the top	Foram	1890 +/− 35	AD 426– 610	**AD 81–399**	AD 560–762	**AD 215–547**
	CALA-05 III 42–43 Poz-34627	Within the coarse base	Foram	7340 ± 50	resedimented			
	CALA-05 III 45.5–47 Poz-34728	Within the coarse base	Foram	10770 ± 70	resedimented			
	CALA-05 III 61.5–62.5 Poz-35778	14 cm below the base	Foram	3195 +/− 30	BC 1170–1932		BC 982–779	
	CALA-05 III 78–79 Poz-34933	32 cm below the base	Foram	5000 ± 35	BC 3496–3327		BC 3342–3047	
	CALA-05 III 87–88 Poz-34934	41 cm below the base – within S1	Foram	6430 ± 40	BC 5091– 4834		BC 4932–4667	
	CALA-05 I 37.5–38.5 Poz-34939	Just below the base of the OLD HAT (pelagic)	Foram	14590 ± 80	BC 15647–14993		BC 15514–14891	
CALA-04 3845 m	Cala 04 VI 45.5–46.5 Poz-35787	23 cm above the top	Foram	905 +/− 30	AD 1384–1490		AD 1470–1651	
	Cala 04 V 4–5 Poz-37402	7 cm above the top	Foram	1405 +/− 30	AD 970–1039		AD 1046–1250	
	Cala 04 V 8–9 Poz-37403	3 cm above the top	Foram	1860 +/− 30	AD 452– 631	**AD 43–380**	AD 598–781	**AD 189–530**
	CALA 04 IV 50 Poz-34629	Within the coarse base	Plant	4800 ± 35	resedimented			
	CALA 04 IV 99–100 Poz-37401	15 cm below the base	Foram	3420 +/− 35	BC 1397–1304		BC 1305–1002	
	Cala 04 III 24–25 Poz-37398	39 cm below the base	Foram	4990 ± 40	BC 3499–3311		BC 3337–3023	
	Cala 04 III 38.5–39.5 Poz-37400	53 cm below the base (S1)	Foram	6690 ± 40	BC 5363–5191		BC 5246–4969	

Measured ages were calibrated according to the radiocarbon calibration program *CALIB REV6.0.0*[53,54] and results are reported both for ΔR = 0(column 6) and ΔR = 147 ± 43(column 8) calculated as the weighted mean including 2 ΔR values from published reservoir ages in the surrounding areas (Calib database at http://calib.qub.ac.uk/marine/). In the discussion we consider only the results with the ΔR = 147 ± 33 but our conclusions would not change considering ΔR = 0 and correlation between HAT emplacement and the Cretan earthquake is confirmed with both ΔR values. Ages of the HAT are reported in column 7 and 9 for ΔR = 0 and ΔR = 147 ± 43 respectively. These ages have been calculated considering the time delay introduced by sampling above the top of the megaturbidite, that is 110 ± 46 (core CALA 05) and 140 ± 46 years (core CALA 04) for each cm above the top (see section Radiometric dating of the HAT in the main text).

tsunamis[38]. However, events such as the Ms 6.60, AD 361 Sicilian and Ms 6.30, AD 374 Reggio Calabria (Table 2) had too low a magnitude to account for the remobilisation of such a large volume of sediments in so wide an area as in the HAT event. These medium magnitude earthquakes can not account for ground peak accelerations required to perturb stability conditions of slope sediments[39] especially 600–700 km away from the epicentre.

The only historical earthquake potentially capable of generating devastating effects in the Ionian Sea, the Sirte abyssal plain and the Herodotus Trough during the given time interval, is the exceptionally strong Cretan 365 AD earthquake[34].

The AD 365 Cretan earthquake occurred on a major reverse fault, dipping beneath Crete and cropping out near the Hellenic Trench. The best fitting model of fault slip (length 100 km, dip 30°, slip 20 m to a depth of about 45 km) calls for an earthquake of magnitude 8.3–8.5[34]. Calculations of tsunamis triggered by this event show an open ocean amplitude of the tsunami wave compatible with that observed and modelled in the 2004 Sumatra tsunami, with presumably similar devastating effects on the coastal regions. According to

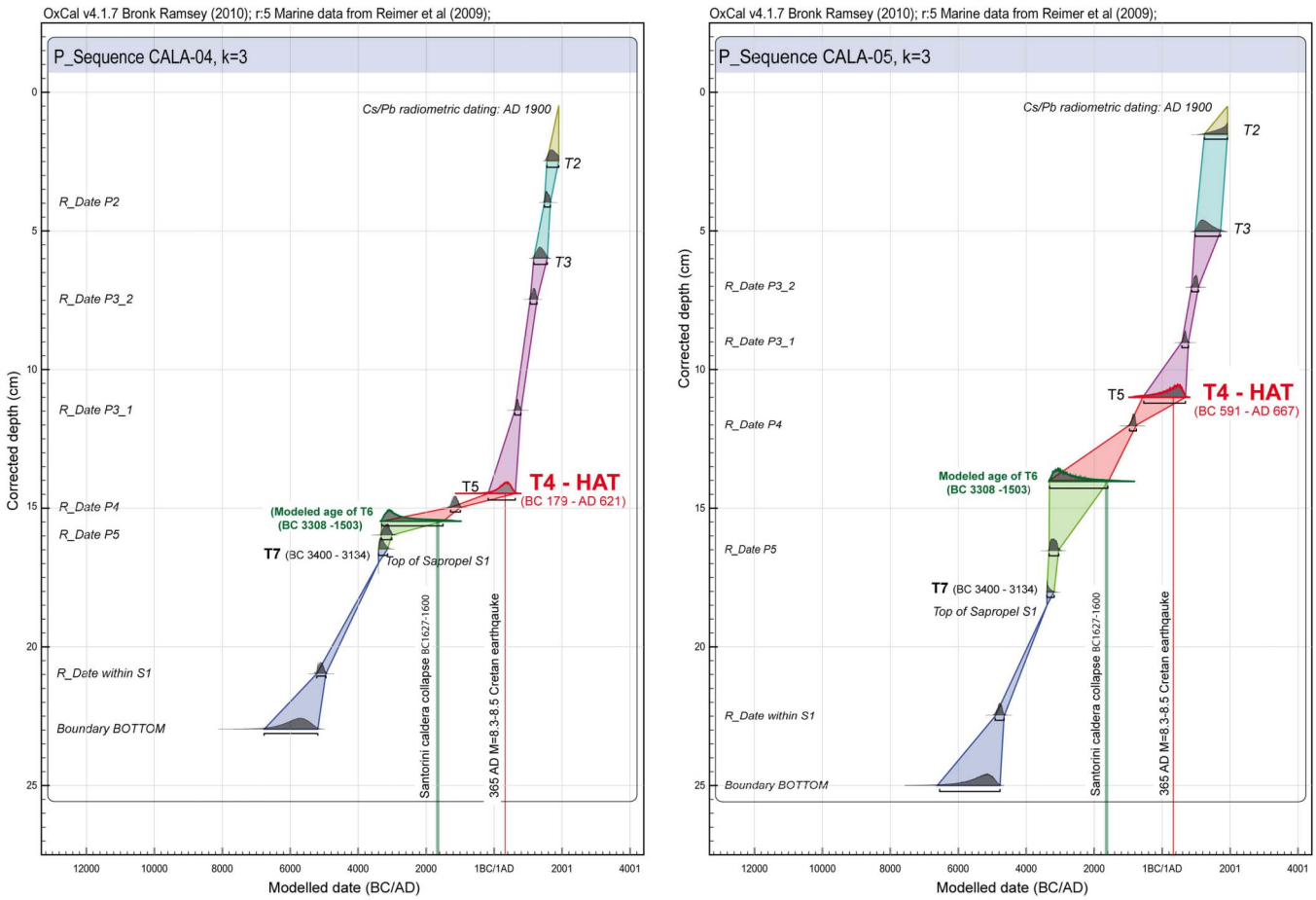

Figure 6 | Age modelling results. Age modelling results obtained for cores CALA 04 (left) and CALA 05 (right) using the P_Sequence (a Bayesian model of deposition) implemented in the computer program OxCal 4.1; this software assimilates sedimentation as a random process following a Poisson law[30]; marine data from (ref 52).The regularity of sedimentation is determined by the k parameter (here k = 3 reflects small variations in sedimentation rate as deduced from radiometric dating analysis). The model finally calculates the age of each corrected depth corresponding to a turbidite and generates the 95.4% probability age ranges (2σ). See Supplementary Material 4 and 5 for further details.

historical records the AD 365 tsunami destroyed cities and drowned thousands of people in coastal areas from Africa, Greece, Sicily and the Adriatic[40].

Earthquake-triggered tsunamis consist of long wavelength/long period water waves, caused by an impulsive vertical displacement of a body of water due either directly to the seismic event, or indirectly to submarine slides. A tsunami wave can trigger overwash surges, backwash flows, debris flows, turbidity currents, bottom currents, etc. These, in turn, will deposit sediment with a variety of depositional mechanisms (sudden freezing, settling from suspension, bed load or traction) resulting in physical features that are not unique to tsunami-induced deposits[41,42].

The powerful pressure pulse resulting from the passage of the tsunami may have caused liquefaction of sediments draping the slopes of the continental margin. The oscillating bottom currents could have stirred sediments into suspension, creating turbulent particle clouds. When the wave hit the steep Malta escarpment it propagated on the shallow and wide continental shelf of the Sicily Channel as well as on the shelf of the Sirte Gulf. The water back-surge eroded extensively the continental shelves triggering gigantic turbidity flows that transported shallow water detritus to the abyssal plain.

The term Augias to indicate the megaturbidite[11] represents well these sedimentary processes. In Greek mythology, Heracles was required to clean in a single day the vast stables of King Augias, which he accomplished by diverting a river and discharging its load into the sea[43]. Similarly, tsunamis triggered by the AD 365 earthquake, cleaned out the Mediterranean shelves.

The HAT geochemical, mineralogical and micropaleontological signatures (Figs. 3, 4 and 5, Supplementary S2 and S3) allowed to reconstruct that the multisource units deposited in response to tsunami waves, backwash flows and related gravity-driven processes are the primary means of downslope sediment transport. In this scenario sediment provenance and related lithofacies provide criteria for identifying paleotsunami deposits[17,42] and turbidite emplacement mechanism. Correlation between HAT composition and onland geology suggest that:

- Unit I derives from the Malta escarpment (it contains carbonates from the Hyblean plateau and minerals from the Etna volcano).

- Unit II contains different sediment sources compatible both with the northern Malta escarpment and southern Calabria/Eastern Sicily

Table 2 | List of likely triggering historical earthquakes

Date	Location	Magnitude	Tsunamigenic
361	Sicily	Ms 6.60	No information
21 July AD 365	Creta	M_w 8.3–8.5	YES
374	Reggio Calabria	Ms 6.30	No information

Major and moderate historical earthquakes known in the study area[35,38,41] in the time window of HAT emplacement as deduced from radiometric dating.

(minerals compatible with the metamorphic basement of southern Calabria and from the Etna volcano).

- Unit III contains material derived from the Sicily Channel as shown by the abundance in foraminiferal assemblages of epiphytic species mainly belonging to Spirillina vivipara (see Supplementary S3); by the isotopic composition of organic matter (Supplementary S8) suggesting relict organic matter of continental origin; and by the presence of cold water species. The back wash surge caused by the tsunami therefore must have eroded sediment deposited during the last sealevel lowstand (LGM) when the Sicily Channel was mostly exposed subaereally[44].

- Units IV and V, composed of fine clay-rich sediments, could be related to the final stage of turbidite emplacement, when the fine suspended load or *"foam"*, settled down from the water column.

Seismic shaking from a single, although large, event, is probably not capable of triggering giant turbidity currents 600–800 km from the epicentre. The analysis of shake maps of an earthquake of similar magnitude (the M = 8.2 April 11 2012 earthquake off the west coast of northern Sumatra[45]) produced peak ground acceleration (PGA) in the order of 0.003–0.028 g about 500 km far from the epicenter. Results from slope stability back-calculations imply PGS's larger than 0.14 g to trigger turbidity currents for sediment strength in the order of 5–6 kPa[39]. Seismic shaking from the Cretan earthquake, although exceptional, was probably unable to trigger mass movements 600–800 km from the epicenter in a flat and stable area of the Sicily channel.

Some of the HAT components are compatible with a source in the inner part of the Sicily Channel, and they suggest that tsunami waves, rather than seismic shaking, mobilized sediments from this region, although far from the epicentre, and carried them into the deep abyssal plain. Tsunami modelling in the Ionian Sea[22] shows that the areas more prone to slope instability are those of the Malta Escarpment, Eastern Sicily and Southern Calabria, that are, in fact, source areas of the HAT, as deduced by our study.

According to simulation models[34], the tsunami wave generated by the 365 AD Cretan earthquake hit orthogonally the edge of the Malta escarpment 70 minutes after the event (Fig. 1); the Malta escarpment is very steep (up to 30°) with a large vertical displacement of the seafloor(>2000 m) relative to the basin floor. The top of the escarpment represents the edge of a wide continental shelf in the Sicily Channel. Therefore, the Malta escarpment must have produced a dramatic impact with the tsunami wave that hit it nearly orthogonally, with amplitude increase and wavelength shortening, reflected in increased shear stress at the seafloor. This scenario could explain why the HAT is recovered mostly in the Ionian and Sirte abyssal plains and the Herodotus trough (Fig. 1), with a maximum thickness of about 25 m[16], while it is absent elsewhere in the Easternmost Mediterranean[46], where the tsunami wave hit the continental margin obliquely, with no vertical relief allowing the wave to cause shear stresses at the seafloor. Nevertheless, according to tsunami model results[34] the city of Alexandria located on the western side of the Nile delta, was devastated by the tsunami wave due to a peculiar coastal topography which favoured the inundation from a wave propagating from the SW parallel to the coastline. The inundation of Alexandria in AD 365 has remained in the historical record as the main disaster following the Cretan earthquake because it was the most populated and flourishing city in the region. Indeed there is historical record of disasters by the tsunami also in other Ionian coastline settlements[40].

Paleo-shoreline observations in Crete suggests that the 365 AD earthquake was the only large seismic event in that region in the past 1650 yrs[34], in agreement with the observation that no other turbidites similar to the HAT are present in the uppermost sedimentary sequence of our cores. Based on GPS deformation rates and estimates of co-seismic slip affecting marine terraces a ~4,500 years recurrence time for AD 365 type earthquakes has been suggested[34].

Only another turbidite bed has been observed in our cores with sedimentological and geochemical characters similar to the HAT. The only other carbonate turbidite observed in our cores lies beneath sapropel S1. This older turbidite is visible in our high-resolution chirp sonar images and shows high lateral continuity and amplitude (Fig. 4). We correlated this layer to the "Deeper Transparent Layer" (DTL)[25], reported to be late Pleistocene, last glacial stage[15]. AMS ^{14}C ages we obtained from pelagic sediments below its base suggest it was emplaced after 14.590 ± 80 yrs BP uncalibrated (Tab. 1). This is the minimum age for this turbidite because an erosive base can not be excluded. This implies that only two events were capable to produce sediment remobilization at the scale of the Mediterranean basin during the last 15,000 yrs.

We conclude that: (a) the HAT was triggered by the tsunami following the AD 365 Cretan earthquake; it remains the only evidence to date of a deep sea tsunami deposit; (b) the HAT contains components from different sources, implying remobilization of material from areas very far from the epicentre; (c) the Santorini eruption might indeed have triggered mass failures in the central Mediterranean, but not the deposition of a megaturbidite; (d) another major megaturbidite, correlated to the regionally recognized DTL acoustic interval, point to a large recurrence time of such extreme sedimentary events which have the Malta escarpment and the Sicily Channel as the source area for sediment remobilisation; (e) more than 90% (93–95%) of the volume of the Holocene and late Pleistocene sediment cover in the Ionian Sea were deposited by turbidity currents mainly triggered by seismic activity (at least during historical times).

Methods

The HAT was studied through an integrated geophysical/geological approach aiming at defining the structure and composition of the deposit recovered in the sediment cores and reconstructing its distribution through the analysis of high resolution geophysical data. Guided by online sub-bottom CHIRP seismic data interpretation, we were able to sample the top and base of the HAT in different sedimentary basins by carefully selecting coring stations in the areas where the homogenite has its minimum thickness.

CHIRP seismic data has been acquired during the 2008 CALAMARE cruise with the R/V CNR Urania using a Benthos Chirp II system equipped with 15 transducers.

Gravity core CALA 05 was collected at 3814 m of water depth in a small basin at about 30 m above the abyssal plain with a 1,2 T gravity corer and analysed through a multidisciplinary approach. Core CALA 04 was collected at 3845 m of water depth in the Ionian abyssal plain. We selected core CALA 05 for a high resolution multidisciplinary study while radiometric dating were performed on both CALA 05 and CALA 04.

Grain size: 184 sediment samples were collected at 1 cm space from core CALA 05 and analysed for grain size distribution using a coulter-counter laser Beckman LS-230 measuring the 0.04–2000 μm fraction at 0.004 μm resolution. Samples were treated with hydrogen peroxide and the disaggregated sediments were re-suspended into a 0.1% sodium-hexametaphosphate solution and left in an ultrasonic bath for 3 minutes. The results were classified according to the[47] grain-size scale.

Magnetic susceptibility was acquired using a Bartinghton model MS2 (100 mm ring) at a sampling rate of 1 cm.

Sediment composition and geochemistry: The sediment chemical composition was obtained using an Avaatech XRF-core scan measuring at 1 cm resolution. The analyses were performed using two instrumental settings at 10 and 50 kV that allow the measurement of sediment's major and minor elements including Al, Si, K, Ti, Ca, Fe, Ba, Zr and Sr. This method allows for a semi-quantitative analysis of the elements content, and the results were normalized to the Ti detrital-phase. In addition, sediments colour indexes were recorded while scanning the cores for high-resolution photographs.

Organic carbon: Forty-six samples were analysed for organic carbon (C_{org}) and total nitrogen (N_{tot}) using a NA-2100 Elemental Analyzer and following the procedure of[48]. The C_{org}/N_{tot} ratio was used to distinguish between marine and continental derived organic matter (OM) according to[28]. 25 key samples were analysed for organic carbon and $\delta^{13}C$ analyses at ISMAR (Institute of Marine Sciences). Analysis were performed on acidified sediment (HCl, 1.5 M) to remove the inorganic fraction. Total carbon (TC), total nitrogen (TN) and $\delta^{15}N$ were determined on untreated sediments. Analyses were performed using a Finnigan DeltaPlus mass spectrometer directly coupled to a FISONS NA2000 Element Analyzer via a CONFLO interface for continuous flow measurements. Inorganic carbon (IC) was estimated by the difference between TC and C_{org}. IC, C_{org} and TN contents are reported as weight percent (wt%), whereas stable isotope data are presented using the conventional delta notation (δ). The average standard deviation of the carbon and nitrogen contents, determined by replicate analyses of the same sample, was ± 0.07 and ± 0.01% (1 SD),

respectively. The internal standards for isotopic measurements were IAEA-CH7 (polyethylene, −32.15‰) and IAEA-N-1 (ammonium sulfate, +0.4‰) for $\delta^{13}C$ and $\delta^{15}N$, respectively. Errors for replicate analyses of the standards were ±0.05‰ and ±0.2‰, respectively.

Mineralogy: mineralogical analyses were carried out on selected key samples to identify main components (minerals, plant fragments) using Polarized Light Microscope (PLM), and scanning electron microscope with EDS attachment (SEM/EDS) on thin sections.

Micropaleontology: analysis were performed on size fraction >63 μm. Eighty-eight samples, 1 cm thick, were obtained from major lithological and grain size changes. The samples were weighed, wet sieved, dried and, when necessary, split into aliquots containing at least 300 specimens of benthic taxa; samples with scarce microfauna have been studied on the entire fraction. Planktonic foraminifera were identified following the taxonomic concept of[49] and semi-quantified, while benthic foraminifera were picked, identified following the taxonomic concept of[50] and counted. We concentrated on benthic foraminifera because each individual taxa has restricted environmental niche that makes this group of organism extremely useful to determine sediment source.

Species were grouped considering their bathymetric distribution: i) "inner shelf" specimens comprise shallow water indicators such as *Ammonia beccarii, A. perlucida, E. advenum, E. crispum, E. decipiens, E. macellum, Gavelinopsis lobatulus, G. traslucens, G. praegeri, G.* sp., *Haynesina germanica, Nonionella turgida, Protelphidium granosum, Valvulineria bradyana* and epiphytes mainly restricted to sandy sub-strata densely vegetated such as *Asterigerinata mamilla, A. planorbis, Astrononion stelligerum, Cibicides lobatulus, Neoconorbina orbicularis, Patellina corrugata, Planorbulina mediterranensis, Rosalina globularis*, and *Spirillina vivipara*; ii) "outer shelf to upper slope" specimens include *Cibicidoides kullenbergi, C. robertsonianus, Trifarina angulosa, Uvigerina auberiana, U. longistriata, U. mediterranea, U. peregrina, U. proboscidea*; iii) "middle to lower bathyal" comprises *Bolivina* spp., *Brizalina* spp., *Cassidulina* sp., and *Gyroidinoides* spp.

Radiometric dating: accelerator mass spectrometry (AMS) radiocarbon dating of handpicked planktonic foraminifera was performed at the Poznań Radiocarbon Laboratory-Foundation of the Adam Mickiewicz University (Poland). We selected samples in the pelagic units bracketing the HAT (Fig. 4 and Table 1). About 5-6 mg of specimens (either mixed or monospecific, when possible, and without evidence of carbonate overgrowth or pyritization) >125 μm in size from 1-cm thick samples were studied. The ^{14}C concentration of the samples is measured in the spectrometer by comparing the simultaneously collected ^{14}C, ^{13}C and ^{12}C beams of each sample with those of Oxalic Acid standard CO_2 and coal background material[51]. Conventional ^{14}C ages are calculated with a $\delta^{13}C$ correction for isotopic fractionation.

The first step to reconstruct the turbidite event chronology was to calibrate the ^{14}C ages of the pelagic sediment samples using the MARINE09.14 calibration curve[52] in CALIB Rev. 6.0 programme[53] applying an average regional reservoir age of $\Delta R = 0$ and $\Delta R = 147 \pm 33$ calculated as the weighted mean including 2 ΔR values from published reservoir ages in the surrounding areas (Calib database at http://calib.qub.ac.uk/marine/) and considering that a mixing between Adriatic and Ionian deep water may be present in the working region. We will consider here only the results with the $\Delta R = 147 \pm 33$. It should be noted that using $\Delta R = 0$ would not affect the main results of this work.

Age modelling: Since the samples of pelagic sediments are located a few cm below the base of the turbidite or some cm above the turbidite tail, it was necessary to interpolate the ages of the calibrated samples to determine the age of each single turbidite. For this purpose we estimated the deposition rate from two successive radiometric dates in the pelagic sequence and we used this information to interpolate the age of the different turbidite beds. Moreover, given the imprecision of individual calibrated radiocarbon determinations it is necessary to use the information we have about the deposition process to refine our chronologies and to provide an interpolation between dated levels in the deposition sequence that takes into account the error propagation[30]. The age model is built using the P_Sequence (a Bayesian model of deposition) implemented in the computer program OxCal 4.1 that assimilates sedimentation as a random process following a Poisson law[30]. The input parameters to generate the P_Sequence model are the uncalibrated ^{14}C ages and respective ΔR with their corresponding corrected depths. The regularity of sedimentation is determined by the k parameter with the higher values of k reflecting smaller variations in sedimentation rate[30]. For our purposes we chose a $k = 3.0$ because we assume that pelagic sedimentation is rather constant in the study area. The model finally calculates the age of each corrected depth corresponding to a turbidite and generates the 95.4% probability age ranges (2σ).

1. Mutti, E., Ricci Lucchi, F., Seguret, M. & Zanzucchi, G. Seismoturbidites: A new group of resedimented deposits. *Marine Geology* **55**, 103–116 (1984).
2. Goldfinger, C. Submarine Paleoseismology Based on Turbidite Records. *Annu. Rev. Marine. Sci.* **3**, 35–66 (2011).
3. Kastens, K. A. & Cita, M. B. Tsunami-induced sediment transport in the abyssal Mediterranean Sea. *Geol. Soc. Am. Bull.* **92**, I, 845–857 (1981).
4. Urgeles, R., Masson, D. G., Canals, M., Watts, A. B. & Le Bas, T. Recurrent, large-scale landsliding on the West flank of La Palma, Canary Islands. *J. Geophys. Res.* **104**, 25,331–25,348 (1999).
5. Garcia-Castellanos, D., Estrada, F., Jiménez-Munt, I., Gorini, C., Fernàndez, M., Vergés, J. & De Vicente, R. Catastrophic flood of the Mediterranean after the Messinian salinity crisis. *Nature* **462**, 778 (2009).
6. Rothwell, R. G., Rothwell, R. G., Thomson, J. & Kähler, G. Low-sea-level emplacement of a very large Late Pleistocene 'megaturbidite' in the western Mediterranean Sea. *Nature* **392**, 377–380 (1998).
7. Ben-Avraham, Z., Woodside, J., Lodolo, E., Gardosh, M., Grasso, M., Camerlenghi, A. & Vai, G. B. Eastern Mediterranean basin systems. *Geological Society, London, Memoirs* **32**, 263–276 (2006).
8. Polonia, A., Torelli, L., Mussoni, P., Gasperini, L., Artoni, A. & Klaeschen, D. The Calabrian Arc Subduction Complex in the Ionian Sea: Regional architecture, active deformation and seismic hazard. *Tectonics* **30**, TC5018 (2011).
9. Kastens, K. A. Earthquakes as a triggering mechanism for debris flows and turbidites on the Calabrian Ridge. *Mar. Geol.* **55**, 13–33 (1984).
10. Hieke, W., Melguen, M. & Fabricius F. Migration of tectonics from the Mediterranean Ridge into the Messina Abyssal Plain (Ionian Sea). *Rapp. Comm. Int. Mer Mèdit* **23**, 4a, 89 (1975).
11. Hieke, W. A. Thick Holocene homogenite from the Ionian abyssal plain (Eastern Mediterranean). *Mar. Geol.* **55**, 63–78 (1984).
12. Hieke, W. & Werner, F. The Augias megaturbidite in the central Ionian Sea (central Mediterranean) and its relation to the Holocene Santorini event. *Sediment. Geol.* **135**, 205 –218 (2000).
13. Stanley, D. J. Unifites: structurless muds of gravity-flow origin in Mediterranean basins. *Geo-Marine Letters* **1**, 2, 77–83 (1981).
14. Cita, M. B., Camerlenghi, A. & Rimoldi, B. Deep-sea tsunami deposits in the eastern Mediterranean: new evidence and depositional models. *Sedimentary Geology* **10**, 155–173 (1996).
15. Cita, M. B. & Aloisi, G. Deep-sea tsunami deposits triggered by the explosion of Santorini (3500 y BP) eastern Mediterranean. In Shiki T., Cita, M. B. & Gorsline D. S. (Eds.), Sedimentary Features of Seismites, Seismo-turbidites and Tsunamites. *Sedimentary Geology* **135**, 1–4, 181–203 (2000).
16. Cita, M. B. & Rimoldi, B. Prehistoric mega-tsunami in the eastern Mediterranean and its sedimentary response. *Rend. Fis. Acc. Lincei* **9**, 16, 137–157 (2005).
17. Shiki, T. & Cita, M. B. Tsunami-Related Sedimentary Properties of Mediterranean Homogenites as an Example of Deep-Sea Tsunamite. In: Tsunamiites-Features and Implications' T. Shiki, Y. Tsuji, T. Yamazaki, and K. Minoura, eds., 203–215. Elsevier, Amsterdam (2008).
18. Cita, M. B., Camerlenghi, A., Kastens, K. A. & McCoy, F. New findings of Bronze Age homogenites in the Ionian Sea: Geodynamic implications for the Mediterranean. *Mar. Geol.* **55**, 47–62 (1984).
19. Troelstra, S. Late Quaternary sedimentation in the Tyro and Kretheus Basins, southeast of Crete. *Mar. Geol.* **75**, 77–91 (1987).
20. Cita, M. B. & Rimoldi, B. Geological and geophysical evidence for the Holocene tsunami deposit in the eastern Mediterranean deep-sea record. *Journal of Geodynamics*, **24**, 293–304 (1997).
21. Rebesco, M., Della Vedova, B., Cernobori, L. & Aloisi, G. Acoustic facies of Holocene megaturbidites in the Eastern Mediterranean. *Sedimentary Geology* **135**, 65–74 (2000).
22. Pareschi, M. T., Boschi, E. & Favalli, M. Lost tsunami. *Geophys. Res. Lett.* **33**, L22608 (2006).
23. Vigliotti, L. Comment on "Lost tsunami" by Maria Teresa Pareschi *et al. Geophys. Res. Lett.* **35**, L02608 (2008).
24. Hieke, W., Hirschleber, H. B. & Dehghani, G. A. The Ionian Abyssal Plain (Mediterranean Sea): morphology, subbottom structures and geodynamic history—an inventory. *Mar Geophys Res* **24**, 279–310 (2005).
25. Hieke, W. Transparent layers in seismic reflection records from the central Ionian Sea (Mediterranean)—evidence for repeated catastrophic turbidite sedimentation during the Quaternary. *Sediment. Geol.* **135**, 89–98 (2000).
26. Mercone, D., Thomson, J., Croudace, I. W., Siani, G., Paterne, M. & Troelstra, S. Duration of S1, the most recent sapropel in the eastern Mediterranean Sea, as indicated by AMS radiocarbon and geochemical evidence. *Paleoceanography* **15**, 336–347 (2000).
27. Polonia, A., Panieri, G., Gasperini, L., Gasparotto, G., Bellucci, L. G. & Torelli, L. Turbidite paleoseismology in the Calabrian Arc subduction complex (Ionian Sea). *G-cubed* (in press).
28. Meyers, P. A. Preservation of elemental and isotopic source identification of sedimentary organic matter. *Chemical Geology* **114**, 289–302 (1994).
29. de Lange, G. J. Early diagenetic reactions in interbedded pelagic and turbidic sediments in the Nares Abyssal Plain (western North Atlantic): consequences for the composition of sediment and interstitial water. *Geochim. Cosmochim. Acta* **50**, 2543–2561 (1986).
30. Bronk Ramsey, C. Deposition models for chronological records. *Quaternary Science Reviews* **27**, 42–60 (2008).
31. Friedrich, W. L., Kromer, B., Friedrich, M., Heinemeier, J., Pfeiffer, T. & Talamo, S. Santorini Eruption Radiocarbon Dated to 1627–1600 B. C. *Science* **312**, 548 (2006).
32. Lorito, S., Tiberti, M. M., Basili, R., Piatanesi, A. & Valensise, G. Earthquake-generated tsunamis in the Mediterranean Sea: Scenarios of potential threats to Southern Italy. *J. Geophys. Res* **113**, B01301 (2008).
33. Polonia, A., Torelli, L., Gasperini, L. & Mussoni, P. Active faults and historical earthquakes in the Ionian Sea. *Nat. Hazards Earth Syst. Sci.* **12**, 2311–2328 (2012).

34. Shaw, B., Ambraseys, N. N., England, P. C., Floyd, M. A., Gorman, G. J., Higham, T. F. G., Jackson, J. A., Nocquet, J.-M., Pain, C. C. & Piggott, M. D. Eastern Mediterranean tectonics and tsunami hazard inferred from the AD 365 earthquake. *Nat. Geosci.* **1**, 268 – 276 (2008).
35. Elias, A., Tapponnier, P., Singh, S. C., King, G. C. P., Briais, A., Daëron, M., Carton, H., Sursock, A., Jacques, E., Jomaa, R. & Klinger, Y. Active thrusting offshore Mount Lebanon: Source of the tsunamigenic A. D. 551 Beirut-Tripoli earthquake. *Geology* **35**, 755–758 (2007).
36. Salamon, A., Rockwell, T., Ward, S. N., Guidoboni, E. & Comastri, A. Tsunami Hazard Evaluation of the Eastern Mediterranean: Historical Analysis and Selected Modeling. *Bulletin of the Seismological Society of America* **97**, 3705–724 (2007).
37. CPTI Working Group. Catalogo Parametrico dei Terremoti Italiani, version 2004 (CPTI04). Istituto Nazionale di Geofisica, Gruppo Nazionale per la Difesa dai Terremoti, Storia Geofisica Ambiente, Servizio Sismico Nazionale, available from: Catalogo Parametrico dei terremoti Italiani, http://emidius.mi.ingv.it/CPTI/ (access: January 10 2013) (2004).
38. Tinti, S., Maramai, A. & Graziani, L. The new catalogue of the Italian tsunamis. *Nat. Hazards* **33**, 439–465 (2004).
39. Strasser, M., Stegmann, S., Bussmann, F., Anselmetti, F. S., Rick, B. & Kopf, A. Quantifying subaqueous slope stability during seismic shaking: Lake Lucerne as model for ocean margins. *Mar. Geol.* **240**, 77–97 (2007).
40. Guidoboni, E., Comastri, A. & Traina, G. Catalogue of ancient earthquakes in the Mediterranean area up to 10th century, 504 pp., Istituto Nazionale di Geofisica e Vulcanologia-Storia Geofisica Ambiente, Bologna (1994).
41. Shanmugam, G. The constructive functions of tropical cyclones and tsunamis on deep-water sand deposition during sea level highstand: implications for petroleum exploration. *AAPG Bull* **92**, 443–471 (2008).
42. Shanmugam, G. Process-sedimentological challenges in distinguishing paleo-tsunami deposits. *Nat Hazards* **63**, 5–30 (2012).
43. Elder, E. *Dictionary of Greek and Roman Biography and Mythology*. In William George Smith (ed), London : J. Walton, I, pp. 168 (1894).
44. Furlani, S., Antonioli, F., Biolchi, S., Gambin, T., Gauci, R., Lo Presti, V., Anzidei, M., Devoto, S., Palombo, M. & Sulli, A. Holocene sea level change in Malta., *Quaternary International* (in press).
45. USGS ShakeMap: off the west coast of Northern Sumatra, Aprile 11 2012, M8.2 earthquake http://earthquake.usgs.gov/earthquakes/shakemap/global/shake/c00090da/(access: January 10 2013).
46. Rothwell, R. G., Reeder, M. S., Anastasakis, G., Stow, D. A. V., Thomson, J. & Kahler, G. Low sea-level emplacement of megaturbidites in western and eastern Mediterranean Sea. *Sedimentary Geology* **135**, 75–88 (2000).
47. Friedman, G. M. & Sanders, J. E. *Principles of sedimentology* (John Wiley & Sons, .New York, , 792 p. (1978).
48. Nieuwenhuize, J., Maas, Y. E. M. & Middelburg, J. J. Rapid analysis of organic carbon and nitrogen in particulate materials. *Marine Chemistry* **45**, 217–224 (1994).
49. Hembleben, C., Spindler, M. & Anderson, O. R. *Modern Planktic Foraminifera. Springer:* 1–363, *New York* (1989).
50. Loeblich, A. R. & Tappan, H. Foraminiferal Genera and Their Classification, 2 v. vanNostrand Reinhold, New York. 970 pp. (1987).
51. Goslar, T., Czernik, J. & Goslar, E. Low-energy 14C AMS in Poznan- Radiocarbon Laboratory, Poland. *Nuclear Instruments and Methods in Physics Research B* **223–224**, 5–11 (2004).
52. Reimer, P. J., Baillie, M. G. L., Bard, E., Bayliss, A., Beck, J. W., Blackwell, P. G., Bronk Ramsey, C., Buck, C. E., Burr, G. S., Edwards, R. L., Friedrich, M., Grootes, P. M., Guilderson, T. P., Hajdas, I., Heaton, T. J., Hogg, A. G., Hughen, K. A., Kaiser, K. F., Kromer, B., McCormac, F. G., Manning, S. W., Reimer, R. W., Richards, D. A., Southon, J. R., Talamo, S., Turney, C. S. M., van der Plicht, J. & Weyhenmeyer, C. E. IntCal09 and Marine09 radiocarbon age calibration curves, 0–50,000 years cal BP. *Radiocarbon* **51**, 4, 1111–1150 (2009).
53. Stuiver, M. & Reimer, P. Extended ^{14}C data base and revised CALIB 3.0 ^{14}C age calibration program. *J. Radiocarbon* **35**, 215–230 (1993).
54. Stuiver, M., Reimer, P. J. & Reimer, R. W. CALIB 5.0. (WWW program and documentation: http://calib.qub.ac.uk/calib/, access 01/23/2013) (2005).

Acknowledgements

We thank the CALAMARE scientific party, Captain V. Lubrano, the officers and the crew of the R/V Urania, and the SOPROMAR for their collaboration in core collection. M. Contessi and F. Petrucci are acknowledged for foraminifera picking for radiometric dating and L. Capotondi for her assistance. We acknowledge H. Nelson for fruitful discussions. The scientific-technical services of the University of Barcelona and ISMAR are acknowledged for XRF and organic carbon analyses. This work has been supported by TOPOMED project.

Author contributions

A.P. conceived and designed the research. A.P. and L.G. acquired data at sea, completed data processing and interpretation. E.B. performed the mineralogical observations and integrated data interpretation. A.C. oversaw the analysis on organic matter. R.L. and A.P. performed sedimentological observations. G.P. carried out micropaleontological analysis. A.P. conceived radiometric dating and age modeling. All authors discussed the problem, methods, analyses and results and reviewed the manuscript. ISMAR paper N. 1782.

Additional information

Supplementary information accompanies this paper at http://www.nature.com/scientificreports

Competing financial interests: The authors declare no competing financial interests.

How to cite this article: Polonia, A. *et al.* Mediterranean megaturbidite triggered by the AD 365 cretan earthquake and tsunami. *Sci. Rep.* **3**, 1285; DOI:10.1038/srep01285 (2013).